Bulletin of Electrical Engineering and Informatics
Vol. 15, No. 6, December 2026, pp. 4774~4791
ISSN: 2302-9285, DOI: 10.11591/eei.v15i6.12777

Iterative single-ended fault location in isolated neutral 6–35 kV networks

Uspanova Anastasia Igorevna[1], Sheryazov Saken Koishybaevich[2], Koshkin Igor Vladimirovich[1], Uspanov Azamat Akhmetuly[1], Utegulov Arman Bolatbekovich[3]
[1]Department of Electric Power Engineering, Faculty of Mechanical Engineering, Energy and Information Technology, Akhmet Baitursynuly Kostanay Regional University, Kostanay, Kazakhstan
[2]Department of Energy Supply and Automation of Technological Processes, Institute of Agricultural Engineering, South Ural State Agrarian University, Chelyabinsk, Russia
[3]Department of Electricity Supply, Institute of Power Engineering, S. Seifullin Kazakh Agrotechnical Research University, Astana, Kazakhstan

Article Info

Article history:

Received Mar 10, 2026
Revised Sep 18, 2026
Accepted Oct 4, 2026

Keywords:

Distributed ABCD model
Distribution networks
Fault location
Isolated neutral
Iterative method
Single-line-to-ground fault

ABSTRACT

This paper proposes an iterative approach for accurate single-line-to-ground (SLG) fault localization in 6–35 kV distribution networks with isolated neutrals. Such faults account for approximately 80% of network disturbances and are typically associated with capacitive fault currents and transition resistances of up to 2000 Ohm. Conventional lumped-parameter representations may result in localization errors of up to 50%, primarily because distributed line capacitance is neglected. The developed approach utilizes an exact ABCD-parameter representation of the line in the zero-sequence domain, where distributed electrical parameters are explicitly considered. A least-squares estimation procedure simultaneously determines fault distance and transition resistance from single-ended voltage and current measurements, accounting for capacitive currents and measurement noise. Monte Carlo analysis yielded an average relative fault-location error of 3.13%, with individual errors ranging from 0.33% to 6.83% across the investigated transition resistance range. Further experimental validation using a 12 km, 35 kV overhead distribution line demonstrated a maximum discrepancy of 0.08 km between simulated and experimental results. Consequently, the proposed iterative approach provides accurate single-ended fault localization without requiring line disconnection, making it highly suitable for reliable fault diagnostics in modern smart-grid distribution systems.

This is an open access article under the CC BY-SA license.

Corresponding Author:

Koshkin Igor Vladimirovich
Department of Electric Power Engineering
Faculty of Mechanical Engineering, Energy and Information Technology
Akhmet Baitursynuly Kostanay Regional University
Kostanay, Kazakhstan
Email: elektroenergetika330@gmail.com

1. INTRODUCTION

Single-line-to-ground (SLG) faults account for approximately 70–80% of disturbances in medium-voltage 6–35 kV distribution networks with isolated neutrals. Under these conditions, the fault current is mainly capacitive, with a phase angle of 75–90°, while the transition resistance (R_F) may exceed 1000 Ohm [1]. Reliable single-ended fault localization without network disconnection is therefore an important operational issue, since prolonged faults can accelerate insulation deterioration, compromise personnel

safety, and develop into phase-to-phase faults. Previous studies can be broadly classified into three methodological groups, whose limitations indicate the research gap considered in this work.

Impedance-based and lumped-parameter techniques remain widely used in practical applications. Ensemble-learning methods [2] and hybrid transient-impedance approaches [3] have demonstrated good performance on IEEE 34-node feeders (24.9 kV) using single-ended voltage and current measurements. However, these methods generally employ lumped π- or T-equivalent models and consequently neglect the distributed capacitance of the line ((C_0)≈5–12 nF/km). For lines exceeding 10 km and transition resistances above 500 Ohm, the reported localization errors can increase to 20–50%. This limitation is particularly significant for isolated-neutral networks, where capacitive components strongly influence the fault current.

Traveling-wave and frequency-domain techniques provide higher spatial resolution. Pathirage *et al.* [4] combines modal propagation delays with Matrix Pencil frequency analysis, whereas [5] applies Transformer-based models to panoramic wavelet representations, achieving section identification rates above 99% and localization errors below 20 m. Despite these results, their practical implementation may require sampling frequencies above 10 kHz, synchronized measurements, or detailed topology encoding. Such requirements limit their applicability to existing 6–35 kV overhead networks with sparse measurement infrastructure. Moreover, these methods do not explicitly account for the low-amplitude, predominantly capacitive zero-sequence currents characteristic of isolated-neutral systems or provide joint estimation of fault distance and R_F.

Since 2020, machine learning (ML) and sparse-estimation approaches have received increasing attention in fault-location studies. Convolutional neural network (CNN)-based techniques using a limited number of phasor measurement units (PMUs) [6], group-sparse modal formulations developed for direct-current (DC) networks [7], and ensemble-learning models have demonstrated resilience to measurement noise and incomplete monitoring [8], [9]. However, most of these data-driven methods are developed and evaluated using lumped-parameter or DC network models, which limits their generalization to AC overhead lines described by distributed parameters, particularly under high transition resistance R_F.

An important exception is the distributed-parameter sparse-estimation method reported in [10]. Instead of using a lumped impedance representation, this approach incorporates exact distributed line equations and formulates the fault-location problem as a nonlinear optimization solved through Lasso and Newton iterations. The results demonstrate that distributed modelling can provide higher localization accuracy than conventional lumped representations. Nevertheless, the method is primarily designed for transmission-level networks and does not consider the specific operating conditions of isolated-neutral distribution systems, including capacitive fault-current phase characteristics. In addition, Monte Carlo evaluation under measurement noise is not addressed, and the proposed scheme relies on multi-terminal measurements or PMU data.

A significant inconsistency can be identified in the existing literature. Lumped-parameter and ML-based approaches frequently report state-of-the-art simulation accuracy, often exceeding 95%, whereas distributed-parameter studies [11]–[13] show that these simplified representations can produce systematic errors of 10–50% when distributed capacitance and high transition resistance become dominant. These conditions are characteristic of 6–35 kV overhead networks with isolated neutrals. Moreover, most published methods either [14], [15] consider grounded or resonant-grounded systems, [16], [17] do not jointly determine fault distance and R_F, [18], [19] require synchronized multi-point measurements, or [20] are validated only on short IEEE test feeders without realistic measurement noise or Monte Carlo analysis. Consequently, no existing approach simultaneously meets the five practical requirements for 6–35 kV isolated-neutral networks: i) complete distributed-parameter ABCD modelling in the zero-sequence domain, ii) single-ended measurements, iii) explicit consideration of the 75–90° capacitive-current phase range, iv) iterative least-squares optimization of fault distance and transition resistance, and v) statistical validation with realistic 1% amplitude and ±5° phase errors.

The present study addresses this gap through an iterative fault-location method employing an exact distributed ABCD-parameter model in the zero-sequence domain. Fault distance and transition resistance are estimated simultaneously from single-ended voltage and current measurements using a least-squares optimization procedure. The formulation incorporates distributed line parameters, capacitive fault-current behavior, and measurement uncertainty. The scientific novelty of the proposed approach is threefold:

a. Methodological: the proposed method integrates a full distributed ABCD matrix in the zero-sequence domain for the specific operating conditions of isolated-neutral 6–35 kV networks with an iterative least-squares procedure for joint estimation of fault distance and (R_F).
b. Practical: fault localization is performed using measurements from a single line end, avoiding the need for synchronized PMUs and dedicated communication channels. This feature is particularly important for aging distribution networks with limited measurement infrastructure.
c. Analytical: the method is assessed through extensive Monte Carlo simulations and full-scale experiments on an actual 12 km, 35 kV overhead line. The results also provide statistical evidence of its robustness to measurement uncertainties of 1% in amplitude and ±5° in phase.

The proposed approach enables accurate fault localization without disconnecting the line and offers a robust and cost-effective solution for smart-grid applications involving aging distribution infrastructure. Its integration into microprocessor-based protection terminals can reduce fault-related outage times, improve personnel safety, and increase the overall reliability of power supply.

2. METHOD

To develop a single-ended fault-location method for 6(10)–35 kV isolated-neutral networks using post-fault operating parameters, an ABCD model (transfer matrix, Figure 1) is established to represent the power line as a four-terminal network with distributed parameters [21]. This representation accounts for the per-unit-length resistance (R), inductance (L), conductance (G), and capacitance (C), which are particularly important in isolated-neutral systems, where the fault current is predominantly capacitive, with a phase angle of 75–90°.

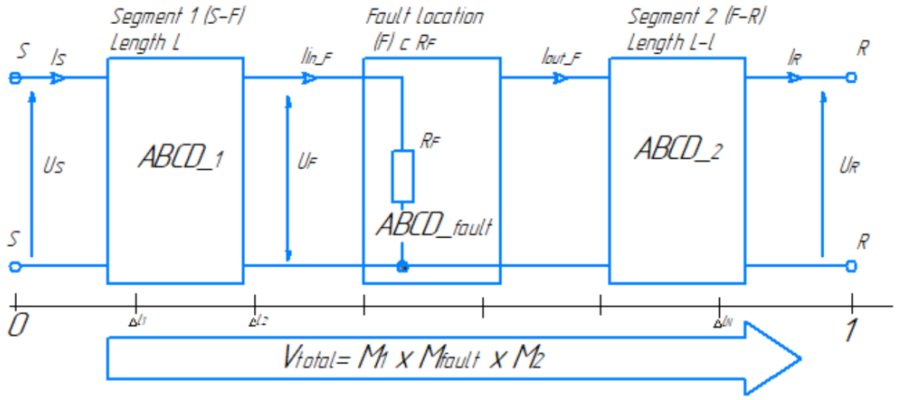


Figure 1. Distributed ABCD matrix for determining the distance to the fault location in a 6(10)-35 kV network with isolated neutral based on emergency mode parameters

In the ABCD representation, the sending-end voltage and current at node (S), denoted by (U_S) and (L_S), are related to the corresponding receiving-end quantities (U_R) and (I_R) at node (R) through the following matrix (1) [22]:

$$\begin{pmatrix} U_s \\ I_s \end{pmatrix} = \begin{pmatrix} A & B \\ C & D \end{pmatrix} \begin{pmatrix} U_R \\ I_R \end{pmatrix}, \quad (1)$$

here, (A) and (D) are dimensionless transmission parameters, (B) has the dimension of impedance (Ω), and (C) has the dimension of admittance (S).

For a distributed-parameter line, the ABCD parameters are obtained from the telegrapher's equations by taking into account the per-unit-length resistance (R), inductance (L), conductance (G), and capacitance (C). The resulting transmission matrix is expressed as [23], [24]:

$$A = \cosh(\gamma L), \quad B = \dot{Z}_c \sinh(\gamma L), \quad C = \frac{1}{\dot{Z}_c} \sinh(\gamma L), \quad D = \cosh(\gamma L), \quad (2)$$

where $\gamma = \sqrt{(R + jwL) \cdot (G + jwC)}$ is the complex propagation constant, which characterizes both signal attenuation and phase variation along the line;

$\dot{Z}_c = \sqrt{\frac{R+jwL}{G+jwC}}$ – is the characteristic (wave) impedance;

where; L denotes the total line length, km; w is the angular frequency, with (w = 2πf) rad/s for a 50 Hz system; and j imaginary unit.

This shows a direct analytical relationship: parameters A, B, C, D are expressed through γ and $\dot{Z}_c$, which depend on specific z_0,y_0. For a zero sequence in emergency mode: $U_0=U_S/3$, $\Delta I_0=\Delta I_S/3$.

The line is divided into two segments: from point S to the fault point F (length l) and from F to R (length L-l), with separate ABCD matrices calculated for each in the zero sequence of symmetrical components (z_0, y_0, γ_0, Zc_0), taking into account the zero voltage $U_0=U_S/3$ and the emergency current component $\Delta I_0=\Delta I_S/3$. The transition resistance R_FF is introduced as a shunt at point F, forming an equivalent resistance $Z_{eq}=R_F||Z_{FR}$ (where Z_{FR} is the input resistance of the second segment, calculated through its ABCD), and the input resistance $Z_{in0}=U_0/\Delta I_0$ is modeled as $Z_{in.расч}=[A_{\{SF\}}\ Z_{eq}+B_{\{SF\}}]/[C_{\{SF\}}\ Z_{eq}+D_{\{SF\}}]$, with the addition of measurement noise (1% on amplitude, ±5° on phase) to create conditions close to real ones.

The iterative process begins with initialization $l_0 \approx I_m(Z_{in0})/I_m(z_0)$ and $R_{F0} \approx 1000$ Ohm, then minimizes the error $|Z_{in.расч}(l, R_F)-Z_{in.meas}|^2$ using the least squares method, with boundaries $0<l<L$ and $R_F>0$, until convergence ($\Delta l<0.1$ km or 50 iterations). This minimizes the influence of R_F (0.... 2000 Ohm), load current, and capacitive nature ($I_C\approx4.8$ A), taking into account the pre-fault mode for ΔI_S.

We use the ABCD matrix, assuming measurements only on S, and approximation of the load on R (Z_R is known or pre-fault). For symmetrical components: we focus on zero ($U_0=Ua/3$, $I_0=Ia/3$ for damaged phase A; $U_b=U_c\approx0$, $I_b=I_c\approx0$).

Step 1: determination of zero sequence parameters.

Specific parameters: $z_0=R_0+j\omega L_0$; $y_0=G_0+j\omega C_0$. Propagation constant: $\gamma_0=\sqrt{z_0\cdot y_0}$, wave impedance: $Z_{c0}=\sqrt{\frac{z_0}{y_0}}$. We use the fault component $\Delta I_s=I_s-I_{load}$, where I_S is the measured current and I_{load} is the pre-fault current. For zero: $\Delta I_0=\Delta I_S/3$, voltage: $U_0=U_S/3$. In the present study these per-unit-length parameters were not taken from reference tables but were measured on the actual test line by the open-circuit and short-circuit method (detailed in Section 3), which avoids the systematic error caused by the mismatch between tabulated and real line parameters.

Step 2: modeling line segments.

ABCD matrix for the segment from S to F (length l):

$$\begin{pmatrix} A_{SF} & B_{SF} \\ C_{SF} & D_{SF} \end{pmatrix} = \begin{pmatrix} \cosh(\gamma_0 l) & Z_{c0}\sinh(\gamma_0 l) \\ \frac{1}{Z_{c0}}\sinh(\gamma_0 l) & \cosh(\gamma_0 l) \end{pmatrix}. \quad (3)$$

For the segment from point F to point R (length L–l):

$$\begin{pmatrix} A_{FR} & B_{FR} \\ C_{FR} & D_{FR} \end{pmatrix} = \begin{pmatrix} \cosh(\gamma_0 (L-l)) & Z_{c0}\sinh(\gamma_0 (L-l)) \\ \frac{1}{Z_{c0}}\sinh(\gamma_0 (L-l)) & \cosh(\gamma_0 (L-l)) \end{pmatrix}. \quad (4)$$

Step 3: equations for determining damage locations, taking into account the distribution across sections of the ABCD matrix.

For the segment from point S to point F:

$$U_0 = A_{SF}U_F + B_{SF}I_{after}, \ \Delta I_0 = C_{SF}U_F + D_{SF}I_{after}, \quad (5)$$

where I_{after} is the current after the S-F section, A;

Next, for the segment from F to R:

$$U_F = A_{FR}U_{R0} + B_{FR}I_{R0}, \ I_{before} = C_{FR}U_{R0} + D_{FR}I_{R0}, \quad (6)$$

where U_{R0} , I_{R0} are the voltage (V) and zero-sequence current (A) at R (for approximation, if Z_R is known: $U_{R0}=-Z_{R0}\cdot I_{R0}$).

Next, a mathematical expression is determined for finding l_{FL}, which describes the process of virtual line scanning. The algorithm sequentially traverses the entire length of the feeder, using the ABCD matrix to convert the U_S voltage and I_S current measured at the substation into U_F and I_F values for each specific point (l). Because the ABCD model incorporates the distributed inductance and capacitance of the line, the procedure accurately accounts for voltage drops and capacitive leakage along the section between the substation busbars and the assumed fault point.

$$l_{FL} = arg\min_{l\in[0,L]}\left(I_m\left[\frac{\Delta\dot{U}_S\cosh(\gamma l)-\Delta\dot{I}_S\sinh(\gamma l)}{\Delta\dot{I}_S\cosh(\gamma l)-\frac{\dot{U}_S}{Z_c}\sinh(\gamma l)-\dot{I}_{rem}(l)}\right]\right)^2, q \quad (7)$$

where $\dot{I}_{rem}$ is the residual line current determined by the load or capacitance state at the terminal node.

The overall computational workflow of the proposed iterative method is presented as structured pseudocode in Figure 2. The procedure comprises four sequential blocks: initialization, objective-function evaluation, Levenberg–Marquardt correction, and boundary-constrained termination. Together, these steps define the computational sequence required to reproduce the proposed method.

Figure 2 presents the least-squares algorithm in pseudocode form. At each iteration, the correction vector $\Delta x = [\Delta l, \Delta R_F]^T$ is obtained by solving the corresponding normal equations using the analytical Jacobian.

The procedure progressively updates the fault distance l_{FL} and transition resistance R_F until the prescribed residual-error tolerance (ϵ) is satisfied. The use of an explicit iterative formulation provides a transparent mathematical description of the optimization process and facilitates independent reproduction of the computational results.

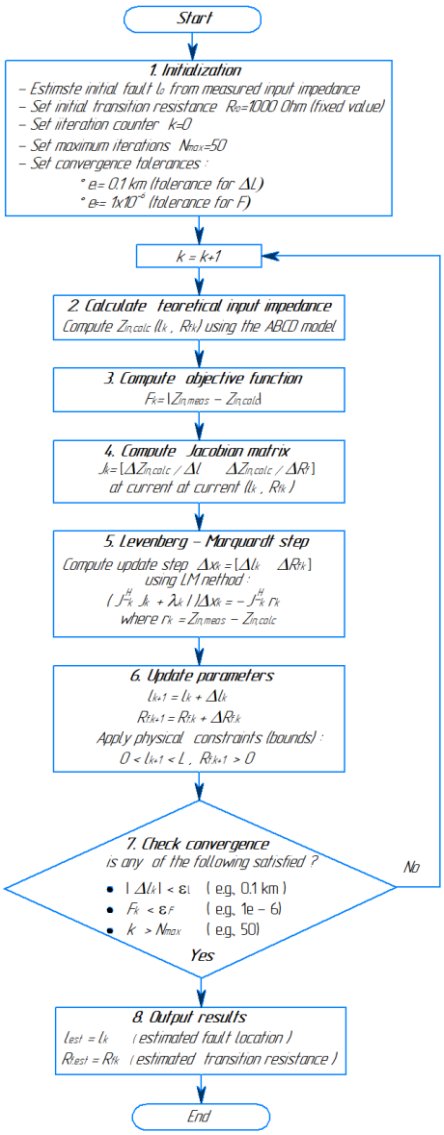


Figure 2. Structured pseudocode of the proposed ABCD-based least-squares fault-location algorithm

The procedure starts with initialization, where initial estimates of the unknown parameters are assigned. The initial fault distance (l_{FL}) is obtained from the imaginary component of the measured input impedance and the zero-sequence line impedance. The initial transition resistance is set to ($R_F = 1000\ Ohms$). This value is physically justified because, at the nominal 50 Hz frequency, the reactive

component of the zero-sequence input impedance increases approximately linearly with distance. Therefore, the corresponding impedance ratio provides a first-order estimate of the fault position with an accuracy of approximately 20–30% even for 1% measurement noise, placing the initial estimate within the convergence region of the global minimum. The selected $R_F = 1000$ Ohms represents the midpoint of the $0 - 2000\ Ohms$ transition-resistance range typical of SLG faults in isolated-neutral 6–35 kV networks [1] and reduces the risk of premature convergence toward either boundary.

The admissible parameter ranges are defined as $0 < l_{FL} < L_0$ and $R_F > 0$. The convergence settings include a distance tolerance of (tol=0.1) km and a maximum of 50 iterations. The iterative procedure stops when the first of the following conditions is met:

- The objective-function residual decreases below $\epsilon \approx 10^{-6}$, indicating numerical convergence of the least-squares solution;
- The change in the estimated fault distance becomes less than (tol=0.1) km, corresponding to the required practical localization accuracy;
- 50 iterations are completed, limiting the computational time to approximately 80–120 ms on a conventional microprocessor-based protection terminal.

The objective function (x) represents the mathematical model of the faulted line. As illustrated in Figure 1, the line is divided into two sections, for which the corresponding ABCD matrices are obtained using the *abcd_matrix(length)* function. For the F–R section, the input impedance Z_{FR} is first determined from the ABCD parameters. The transition resistance R_F is then connected in parallel with Z_{FR} to obtain the equivalent impedance Z_{eq}. Based on this equivalent circuit, the total input impedance seen from the source S, $Z_{in.calc}$, is calculated. The objective function is defined as the squared discrepancy between the measured and calculated input-impedance values.

The parameter estimation is performed using the Levenberg–Marquardt algorithm. At each iteration, the current objective-function value is evaluated and compared with the convergence threshold $\epsilon \approx 10^{-6}$. If the required criterion is not satisfied, the Jacobian with respect to the unknown variables l_{FL} and R_F is evaluated either analytically or numerically. The correction vector (Δx) is then calculated using the damping factor (λ), after which the parameter vector is updated subject to the prescribed physical bounds. The iterations continue until the change in the estimated fault distance (l) falls below the tolerance (tol), or the maximum number of iterations is reached.

After convergence, the algorithm provides the estimated fault distance (l_{FL}) and transition resistance (R_{Fest}). These parameters constitute the solution of the inverse problem and provide the basis for determining the fault position along the power line.

The physical basis of the proposed criterion follows from the predominantly resistive nature of the fault path at the actual fault point. The arc or conductive connection to ground through (R_F) is assumed to have negligible reactance. Consequently, at the correct fault location, the calculated fault voltage (U_F) and current (I_F) should be approximately in phase, and their ratio, defined as the fault impedance (Z_{fault}), should have a minimum reactive component. Therefore, the location corresponding to the minimum value of ($I_m(Z_{fault})$) is taken as the estimated fault position.

The squared discrepancy is used to obtain a smooth non-negative objective function suitable for numerical optimization. As a function of the assumed fault distance (l_{FL}), this criterion forms a minimum near the physically correct solution. The position of this minimum provides the estimate of the fault location, while the corresponding optimized value of (R_F) represents the transition resistance.

3. RESULTS AND DISCUSSION

Based on (7), the fault distance was evaluated using the ABCD matrix, symmetrical components, and distributed line parameters, including the specific impedance (z_0), admittance (y_0), propagation constant (γ_0), and characteristic impedance (Z_{C0}). The model also incorporated the line capacitance ($C_0 \approx 8\ nF/km$) and the fault conditions: source voltage $U_S = 35\ kV$, load current ranging from 15.93 to 62.67 A, and transition resistance R_F varying from 0 to 2000 Ohm. Numerical experiments were conducted in Python using the NumPy, cmath, and SciPy optimization libraries to iteratively minimize the least-squares error. The line length was set to (L=20) km, with the actual fault position fixed at ($l_{true} = 10$) km. The equivalent receiving-end impedance was $\dot{Z}_{R0} = 100 + j50$ Ohms, while the initial load-current component was ($I_{load} = 15.93$) A.

To evaluate the effect of measurement uncertainty in the input impedance (Z_{in0}) on the accuracy of the estimated parameters, a Monte Carlo analysis [25] was conducted using 100 realizations for each test case. Gaussian noise with a standard deviation of 1% was independently introduced into the real and imaginary components of Z_{in0} to represent measurement uncertainty. For all 100 realizations, the iterative optimizer achieved a 100% convergence rate: each run terminated within the prescribed limit of 50 iterations

and satisfied the residual criterion ($\epsilon \approx 10^{-6}$), without reaching either boundary of the admissible fault-distance interval ((l=0) or (l=L)). Depending on the line length and transition resistance (R_F), convergence required an average of 12–18 iterations, demonstrating the computational efficiency of the Levenberg–Marquardt procedure and its potential for real-time implementation.

The zero-noise limiting case is also inherently included in the analysis. Within the fractional factorial design, the central points with (x_2=0) and (x_3=0) represent noise-free measurements, for which the localization error is reduced to the numerical tolerance of the optimization procedure (($\Delta l \leq 0.1$) km), corresponding to less than 0.5% for all considered line lengths. The monotonic increase in (δ_{avg}) and (σ) from the central points toward the factor extremes therefore characterizes the degradation caused by measurement noise. At the same time, the noise-free results indicate that the proposed method is limited primarily by the prescribed numerical/discretization tolerance rather than by a systematic localization bias.

Specifically, the noisy input impedance in the ii-th run was generated as $Z_{in}^{(i)} = Z_{in}^{true} + \varepsilon_{R_e}^{(i)} + j\varepsilon_{I_m}^{(i)}$, where $\varepsilon_{R_e}^{(i)} \sim N(0, \sigma^2)$ and $\varepsilon_{I_m}^{(i)} \sim N(0, \sigma^2)$ are independent zero-mean Gaussian variables with standard deviation $\sigma = 0.01 \cdot \|Z_{in}^{true}\|$. The real and imaginary noise components were assumed mutually uncorrelated, which is justified by the orthogonality of in-phase and quadrature components after discrete Fourier transform processing of the measured signals. Noise samples were also assumed statistically independent across the 100 Monte Carlo runs, modelling a sequence of independent fault events. The resulting composite error corresponds to approximately 1% in amplitude and ±5° in phase, consistent with the accuracy class of the instrument transformers used in the physical experiment. The analysis of the influence of line length L (with damage in the middle and R_F=1000 Ohm) is presented in Table 1.

Table 1. Results of sensitivity analysis using Monte Carlo simulation

Line length L (km)	Mean relative error δ_{avg} in L_{calc} (%)	Standard deviation σ (%)	95%C1=±1.984·$\sigma/\sqrt{N}$
10	7.98	3.14	±0.062
20	5.35	2.59	±0.103
30	4.41	1.37	±0.082
40	3.09	1.29	±0.103
50	2.11	0.94	±0.094

The average relative fault-location error is calculated as (8):

$$\delta_{avg} = \left|\frac{L_{calc} - L_{FL}}{L}\right| \cdot 100\%, \quad (8)$$

where (L_{calc}) is the estimated fault distance obtained from the iterative optimization using the noisy measured input impedance (Z_{in}), (L_{FL}) is the actual fault distance, and (L) is the total line length.
The standard deviation (σ) is calculated as [9]:

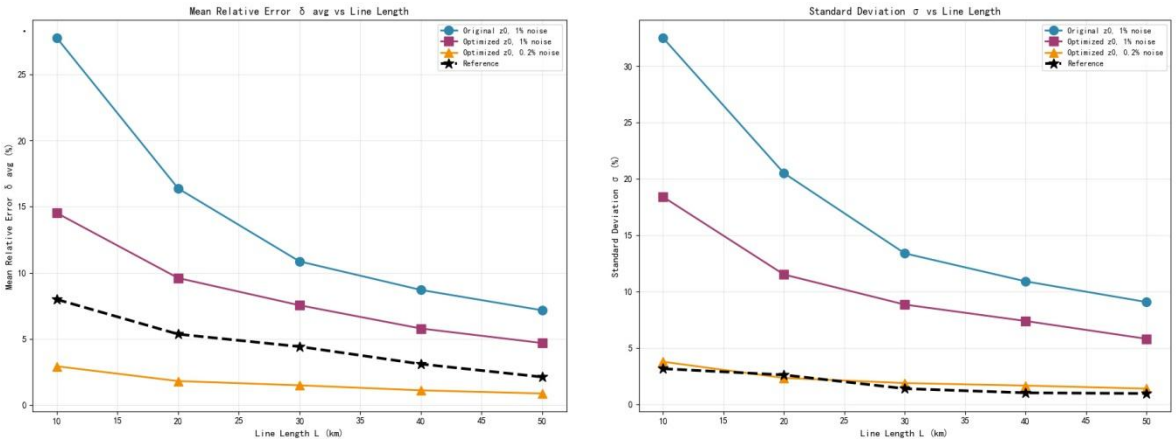
$$\sigma = \sqrt{\frac{1}{N-1}\sum_{i=1}^{N}(l_{calc.i} - \hat{l}_{calc})^2}, \quad (9)$$

where (N) is the number of Monte Carlo realizations, ($l_{calc.i}$) is the estimated fault distance obtained in the (i)-th realization, in km, and ($\hat{l}_{calc}$) is the mean estimated fault distance over all realizations, in km. The use of (N-1) in the denominator corresponds to the unbiased sample standard deviation.

In addition to the point estimates, the 95% confidence interval (CI) for the mean estimated fault distance is calculated as $CI_{95} = l_{calc} \pm \frac{t_{0.975,99}\sigma}{\sqrt{N}}$ where $t_{0.975,99} \approx 1.984$ is the student's critical value for N−1=99 degrees of freedom; this interval quantifies the statistical uncertainty of the estimator at the standard significance level α=0.05.

The simulation results are presented in Figure 3, which contains two complementary panels: Figure 3(a) the mean relative fault-location error (δ_{avg}) and Figure 3(b) the standard deviation (σ), both shown as functions of line length. Both metrics exhibit a consistent decreasing trend as (L) increases from 10 to 50 km. This behavior can be explained by the distributed-parameter representation of the line. With increasing line length, the influence of the receiving-end equivalent impedance (Z_{R0}) on the sending-end input impedance (Z_{in}) decreases, thereby reducing the dependence of the fault-location estimate on the load parameters. As a result, the relative sensitivity of (Z_{in}) to the fault coordinate becomes more pronounced. The statistical behavior of the proposed optimization procedure is further illustrated in Figure 4 for the base

case (L=20 km, l_{true}=10 km). The histogram of the (N=100) fault-location estimates exhibits an approximately Gaussian distribution centered close to the true fault distance. The concentration of the estimates around (l_{true}), together with the corresponding mean error and standard deviation, indicates stable behavior of the estimator under additive measurement noise.



(a) (b)

Figure 3. Statistical analysis results of fault location accuracy using the Monte Carlo method versus line length, showing; (a) mean relative error (δ_{avg}) and (b) standard deviation of the estimate (σ) across different model parameterization scenarios and effective measurement noise levels

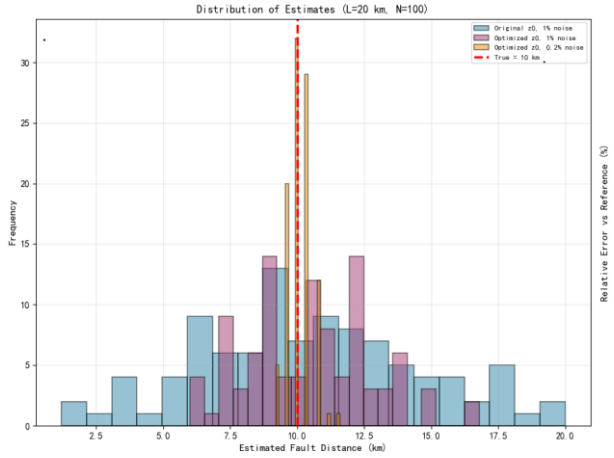


Figure 4. Monte Carlo distribution of fault-location estimates (N=100) for L=20 km and $l_{true} = 10$ km

Figure 4 presents the empirical distribution obtained from the 100 Monte Carlo realizations for the base case. The close agreement between the mean estimated fault distance and (l_{true}) indicates that no pronounced systematic localization bias is introduced by the proposed iterative minimization procedure under the considered noise conditions.

The concentration of the estimates within a relatively narrow confidence interval, with its width determined by the variance of the measurement noise, indicates a high degree of robustness of the least-squares procedure to additive perturbations in the voltage and current measurement channels. The observed scatter is therefore consistent with the random component of the measurement uncertainty rather than with numerical instability or premature convergence to an undesired local solution. Together with the stable convergence behavior observed across the Monte Carlo realizations, these results demonstrate the statistical stability and robustness of the proposed fault-location method under the considered measurement-noise conditions.

Figure 5 summarizes the fault-location results obtained with the distributed-parameter ABCD model. The figure relates the transition resistance (R_F), calculated current phase angle, voltage (U), mean estimated fault distance (l_{calc}), and standard deviation (σ). Here, the subscript "calc" denotes the estimated value returned by the computational model. Only simulation cases satisfying the prescribed current-phase condition of (75-90°), characteristic of the predominantly capacitive fault current in the considered isolated-neutral network, were retained for further analysis.

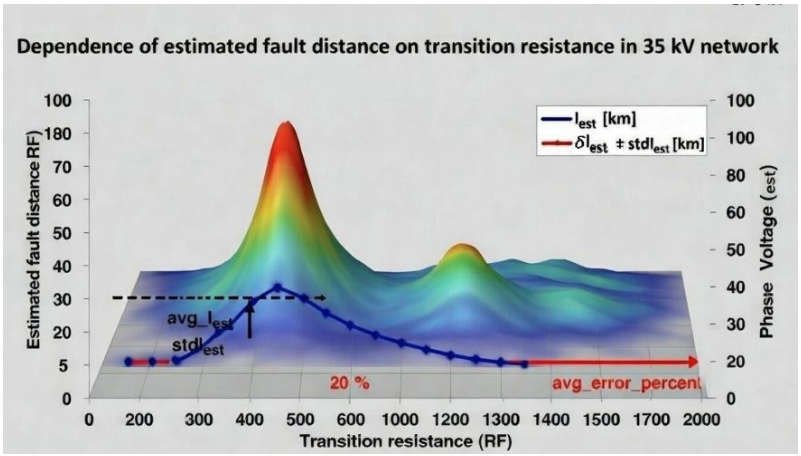


Figure 5. Monte Carlo results for fault-location estimation under varying parameters

The numerical study was based on the distributed-parameter ABCD formulation and the mathematical models established in the preceding sections. Measurement uncertainty was represented by 1% amplitude noise and a phase error of ($\pm 5°$), while the fault parameters were estimated through iterative optimization. For visualization, a reduced parameter set was adopted: (R_F) from 0 to 2000 Ohms at six levels, (U) from 2000 to 8000 V at three levels, and (N=10) Monte Carlo realizations for each parameter combination. The line capacitance was set to ($C = 3e^{-7}$) F/km, providing fault-current phase angles of approximately ($\approx 73 - 85°$) for the considered voltage range, with current magnitudes of approximately 4–5 A at (U=5000) V. To ensure consistency with the specified operating condition, cases with a calculated phase angle below (75°) were excluded from the final dataset.

The robustness observed for capacitive fault currents of 4–5 A with phase angles of 75–90° is primarily associated with the difference between distributed and lumped representations of the zero-sequence network. In isolated-neutral feeders longer than 10 km, the capacitive charging current is distributed continuously along the line rather than represented by a single concentrated element. Lumped π- or T-equivalent models approximate this effect using a single shunt branch, which can introduce a systematic phase error between the actual and calculated zero-sequence current at the fault location. This error increases with line length and consequently affects the impedance-based fault-distance estimate. The proposed approach avoids this simplification by using the telegrapher's equations in their distributed form, with the propagation functions (cosh(γol)) and (and sinh(γol)). Thus, the spatial distribution of the capacitive current is retained for different line lengths and fault positions.

Further stabilization is achieved through the joint least-squares estimation of fault distance and transition resistance. Under predominantly capacitive fault-current conditions, the reactive component of the measured impedance is strongly influenced by the distributed line capacitance and cannot be attributed solely to the fault path. The iterative optimization separates these effects by associating the distance (l) primarily with the reactive component of (Z_{in}), while (R_F) mainly affects its active component. This separation reduces the influence of the capacitive component on the distance estimate and helps maintain localization errors below 10% even for phase angles approaching 90°, where conventional single-parameter impedance methods may exhibit substantial degradation.

The results indicate that the estimated fault distance fluctuates around the actual value of 10 km, while the standard deviation of the estimates varies from approximately 3 to 10 km, reflecting the effect of measurement noise. The mean relative fault-location error, shown by the avg_error_l_percent curve, ranges from 0% for ideal conditions to 36% for low voltage (U) and specific values of (R_F), with typical values of about 5–15%. The error tends to increase as (U) decreases: at (U=8000) V, the localization error is generally

lower than at (U=2000) V. This behavior is attributed to the increasing relative contribution of measurement noise at lower signal levels and, consequently, to the reduction in the effective signal-to-noise ratio.

As (R_F) increases from 400 to 2000 Ohms, accompanied by an increase in the current phase angle from 77.8° to 85.1°, the mean estimated fault distance remains close to the actual value of 10 km, although the dispersion of the estimates increases, with (σ) reaching approximately 8–9 km in the corresponding cases. These results indicate that the proposed method remains applicable at high transition resistances, where the fault current becomes increasingly capacitive and its phase approaches 90°. The influence of (R_F) is accounted for through the joint optimization procedure. For ($R_F \leq 400$ Ohm), the current phase falls outside the specified 75–90° range and becomes less predominantly capacitive, which may adversely affect localization accuracy. Within the 75–90° phase range, the method demonstrates stable performance, with an average error below 10% for ($R_F > 1000$ Ohm) over the considered voltage range. The observed performance at high transition resistance can be attributed to three interrelated physical and mathematical factors.

First, as (R_F) increases, the fault-current magnitude decreases substantially, from approximately 5 A at ($R_F = 0$) to below 1 A at ($R_F = 2000$ Ohm), while the phase angle approaches 90°, indicating an increasingly capacitive current. Consequently, the zero-sequence response becomes more strongly influenced by the distributed capacitance of the line than by the fault-path impedance. The proposed ABCD formulation accounts for this behavior through the propagation constant (γ_0) and characteristic impedance (Z_{C0}), both of which are determined by the distributed line parameters, including the capacitance (C_0). By comparison, simplified lumped-parameter models represent the line using concentrated elements and therefore cannot fully reproduce the spatial distribution of capacitive current along the feeder.

Second, the joint least-squares formulation contributes to the stability of the estimation at high (R_F). Because the transition resistance is included as an optimization variable rather than specified in advance, the algorithm simultaneously updates (l) and (R_F) to reduce the mismatch between the measured and calculated impedance. At high transition resistance, the contribution of the fault branch to the overall admittance becomes smaller, which can reduce variations in the objective function and simplify identification of its minimum. This behavior is consistent with the observed stabilization of the optimization procedure at moderate transition resistances, where a relatively broad low-error region is observed for (R_F) values up to approximately 1200 Ohm.

Third, the physical interpretation of the imaginary-part minimization criterion becomes more pronounced at high (R_F). Since the fault path is assumed to be predominantly resistive, with negligible reactance associated with the arc or ground contact, the condition ($Z_{fault} \rightarrow 0$ is more closely approached when the fault current is small and predominantly capacitive. At lower (R_F), the higher fault-current magnitude produces larger voltage drops along the line, affecting the phase relationship between voltage and current and making the zero crossing of Im(Z_{fault}) less distinct. As a result, the uncertainty of the estimated fault distance may increase.

The proposed iterative method based on the distributed ABCD model was further validated using a fractional factorial physical experiment, since evaluating all possible combinations of the selected factors would require substantially greater computational and experimental resources. A (2^{k-p}) fractional factorial design was adopted, where (k) denotes the number of factors and (p) defines the degree of fractionation. Four significant factors ((k=4)) and (p=1) were selected, resulting in ($2^{4-1} = 8$) experimental runs instead of the 16 required for a full factorial design. The experiments were performed at the university test site under conditions representative of a 12-km, 35-kV overhead line, with the fault introduced at a distance of 6 km (Figure 6). This experimental design makes it possible to account for measurement variability and evaluate the statistical stability of the proposed fault-location method under conditions close to practical operation.

The main experimental factors were selected according to their expected influence on the parameters of the faulted operating condition, based on the preceding Monte Carlo analysis for isolated-neutral networks. These factors affect the accuracy of fault-location estimation through the capacitive fault current, measurement uncertainty, transition resistance, and variation of the distributed line capacitance.

- (x_1): transition resistance R_F (Ohms). The factor varies from 0 Ohm, corresponding to an approximately metallic fault, to 2000 Ohm, representing a high-resistance ground fault, with a central value of 1000 Ohm. Changes in (R_F) affect the fault-current phase angle, the input impedance (Z_{in}), and consequently the accuracy of the estimated fault distance.
- (x_2): measurement amplitude error (relative units). The factor ranges from (-0.01) to (+0.01), corresponding to an amplitude uncertainty of ±1%, with a zero-centered Gaussian distribution. This uncertainty reduces the effective signal-to-noise ratio and may increase the optimization error, particularly at low voltage levels.

- (x_3): measurement phase error (°). The factor varies from (-5°) to (+5°), with a central value of (0°). This factor represents phase uncertainty in the measured signals and is particularly relevant for the predominantly capacitive fault-current conditions considered in this study.
- (x_4): relative variation of the specific line capacitance (C_0). The factor is varied within (-0.2) to (+0.2), corresponding to ±20% around the nominal value. This factor represents possible spatial and operating variations in the distributed capacitance associated with line inhomogeneity and environmental conditions and is particularly relevant to the distributed-parameter model.

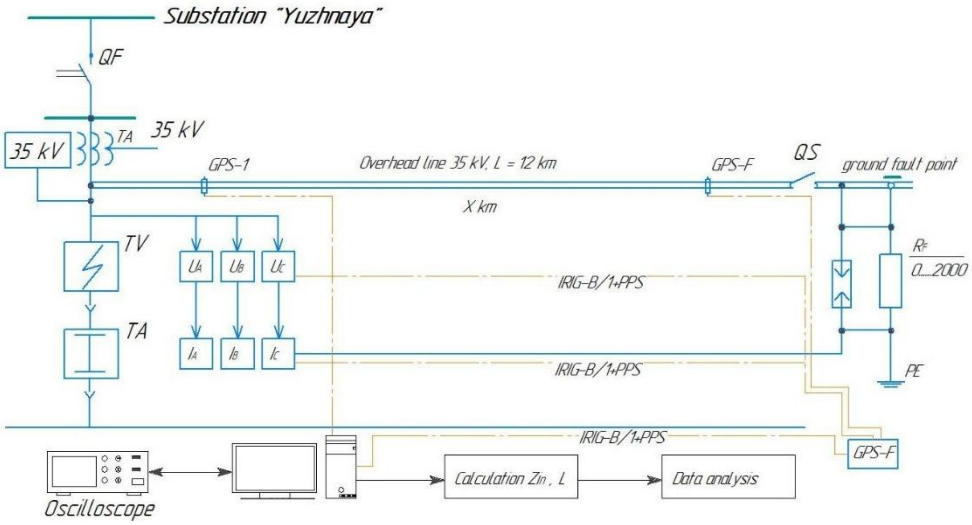


Figure 6. Experimental setup at the University Test Site for a 35 kV ground-fault test based on the distributed ABCD mode

The factors (x_2) and (x_3), representing amplitude uncertainty of ±1% and phase uncertainty of ±5°, respectively, jointly characterize the sensitivity of the proposed method to measurement errors. The obtained results provide an estimate of the permissible measurement-error range for practical implementation and indicate that the method remains stable under the considered uncertainty levels.

Several parameters were not varied and were instead fixed at their nominal values because their contribution to the final fault-location error was considered insignificant. Thus, the specific zero-sequence resistance (r_0) and reactance (x_0) were treated as constant parameters. For lines longer than 10 km, the distributed capacitive coupling has a stronger effect on the fault response, while variations of (x_0) within ±5% produce no significant change in the localization results.

The specific zero-sequence conductance (g_0) was neglected because of its very small magnitude (($\approx 10^{-8}$) S/km, while the system frequency (f) was fixed at 50 Hz. The load current (I_{load}) was set to the representative value of 15 A. The applied zero-sequence formulation is not directly affected by symmetrical load-current components, allowing the load current to be fixed for the basic verification case. The fault distance (L_{FL}) was set to 6 km, corresponding to the midpoint of the 12 km test line. This position provides a representative operating point for evaluating algorithm convergence without introducing additional complexity at the initial sensitivity-analysis stage.

A 2^{4-1} fractional factorial design with generator (D=ABC) was used. This is a resolution IV design, allowing the main effects to be estimated without aliasing with two-factor interactions. The experimental plan comprised three types of points:

- Factorial points: 8 runs (2^{4-1});
- Axial points: 8 runs, with (\pm\alpha) for one factor and the remaining factors set to zero;
- Central points: 6 replicates, used to estimate experimental variance and assess model adequacy.

The use of a fractional factorial design 2^{4-1} (8 experiments) made it possible to effectively identify the dominant influence of R_F transition resistance and measurement noise on the accuracy of determining the distance to L_{FL} damage. Stochastic modeling using the least squares method and three repetitions of the experiments confirmed the high accuracy of the algorithm (error 0–4%) under moderate interference and $R_F > 1000$ Ohm, However, the identified sensitivity to extreme values of factors and the risk of the

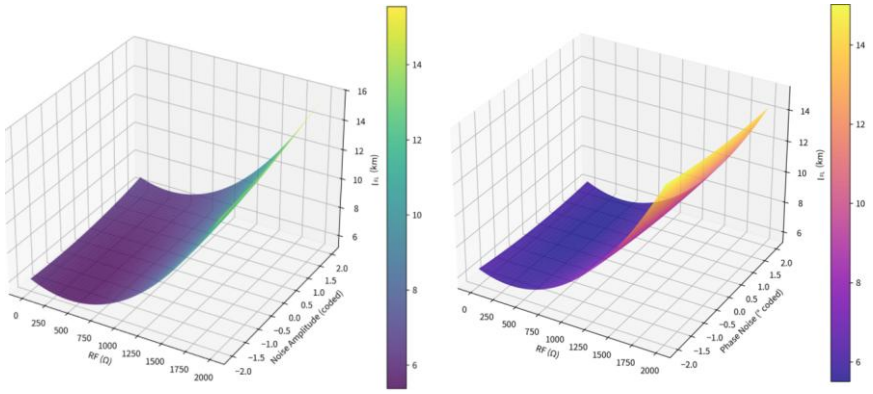
optimizer "sticking" to the boundaries of the range justify the need to introduce regularization of the objective function for reliable industrial implementation of the method.

A second-order regression model including two-factor interactions was fitted in coded variables for the fractional factorial design:

$$L_{FL} = 6.312 + 2.184x_1 + 0.147x_2 - 0.092x_3 - 0.105x_4 + 1.873x_1^2 + 0.068x_2^2 + 0.041x_3^2 + 0.053x_4^2 + 0.124x_1x_2 - 0.081x_1x_3 + 0.139x_1x_4 - 0.047x_2x_3 + 0,076x_2x_4 - 0.058x_3x_4) \quad (10)$$

Response surfaces were then generated from the regression model with the remaining factors fixed at their central values. Figure 7 presents these response surfaces, illustrating the combined effect of transition resistance (R_F) with the two dominant measurement-uncertainty factors. Specifically, Figure 7(a) shows the interaction between (R_F) and amplitude error (x_2). The localization error remains below 4% for $R_F < 1000$ Ohm and low amplitude noise, but increases at ($R_F > 1500$ Ohm), indicating greater sensitivity to measurement perturbations as the fault current decreases.

Figure 7(b) presents the effect of (R_F) and phase error (x_3). The error remains relatively low up to (R_F~1200 Ohm), but increases with phase uncertainty because the current phase is a key indicator of the capacitive fault-current behavior. Figure 8 shows the interaction between (R_F) and the relative variation of (C_0). The method remains largely insensitive to a ±20% variation in (C_0), with a noticeable error increase only for ($R_F > 1800$ Ohm) combined with positive capacitance deviation. This result indicates that the iterative optimization can compensate for moderate uncertainty in distributed line parameters.



(a) (b)

Figure 7. Response surfaces; (a) "R_F ↔ amplitude noise" (x_3=0, x_4=0) and (b) "R_F ↔ phase noise" (x_2=0, x_4=0)

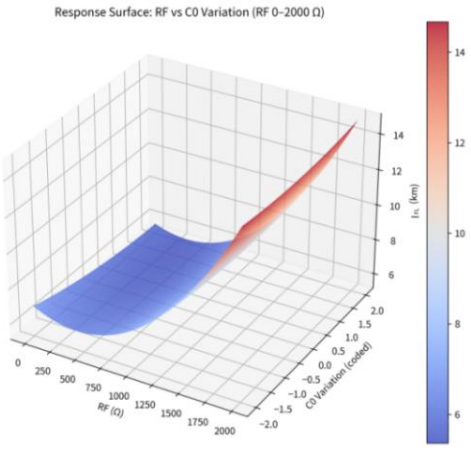


Figure 8. Response surface "R_F ↔ C_0 variation" (x_2=0, x_3=0)

The next stage of the statistical analysis involves testing the homogeneity of variances using Cochran's C test. The test is used to verify the equality of reproducibility variances across all points of the

factor space, which is necessary to ensure the adequacy of the subsequent regression model and the validity of OLS parameter estimates.

Each of the eight factor combinations was tested with an equal number of experiments ((m=3), (f=2)), allowing anomalous variance values to be identified. The calculated Cochran criterion (C_{calc}), defined as the ratio of the maximum partial variance to the sum of all variances, was compared with the critical value (C_{crit}) at the significance level ($\alpha = 0.05$).

For each of the (k=8) experimental groups, the sample variance (S_i^2) was calculated from (m=3) measurements ((f=2)) using [10], [14]:

$$S_i^2 = \frac{1}{m-1} \cdot \sum_{j=1}^{m} \left(y_{ij} - \bar{y}_i\right)^2 \quad (11)$$

where (y_{ij}) is the (j)-th measurement in the (i)-th group and ($\bar{y}_i$) is the corresponding group mean.

For the (L_{FL}) data with (\sigma=0.1), the calculated variances were S_i^2 = [8.15, 13.48, 8.40, 8.05, 10.40, 8.99, 10.24, 7.63].

The Cochran (G) statistic was then calculated according to [10], [14]:

$$G = \frac{\max(S_i^2)}{\sum_{i=1}^{k} S_i^2} = \frac{13.48}{75.14} \approx 0.179 \quad (12)$$

where for the experimental data: $\max(S_i^2)$=13.48, and $\sum S_i^2$=8.15+13.48+8.40+8.05+10.40+8.99+10.24+7.63=75.14.

The hypothesis of homogeneity of variances is confirmed if the calculated value of the G criterion does not exceed the critical (tabulated) value G_{cr} for the given parameters α , k , f otherwise, the variances are considered heterogeneous, and the null hypothesis is rejected. The tabulated values of G_{cr} are taken from Cochran's standard tables (for α=0.05, upper level of significance). For our case (k=8, f=2), $G_{kp} \approx 0.516$ (from standard Cochran's C tables). Below is the relevant part of Table 2 for α=0.05 and f=2 (df=2) for different numbers of groups k (from 2 to 12).

Table 2. Resulting critical values according to Cochran's criterion

Number of groups (k)	2	3	4	5	6	7	8	9	10	11	12
G_{cr} (α=0.05)	0.975	0.871	0.768	0.684	0.616	0.561	0.516	0.478	0.445	0.419	0.395

For k=8, the calculated Cochran criterion G=0.179 is below the critical value $G_{cr} = 0.516$ at ($\alpha = 0.05$), confirming variance homogeneity and supporting the validity of the OLS regression model.

The method was validated experimentally on a 12 km, 35 kV overhead line with an isolated neutral, using an ACSR-70/11 conductor, PS-70 glass insulators, and a BIL of 170 kV. The transition resistance (R_F) was emulated using a calibrated PEV-500 resistor bank (±3% tolerance), verified before each test with a class-0.2 micro-ohmmeter. Each test was repeated three times. Distributed zero-sequence parameters were determined experimentally by open- and short-circuit tests using a P525 Schering bridge (class 0.5), yielding (C_0=7.8±0.3) nF/km, (L_0=3.15±0.08) mH/km, and r_0=0.44±0.02 Ohm/km at 50 Hz. These measured parameters were directly used in the ABCD model, avoiding uncertainty associated with tabulated values.

Zero-sequence voltage U_0 and current ΔI_0 were measured at the sending end using a NAMI-35 voltage transformer and a TOL-35 current transformer (both class 0.5, IEC 61869). The signals were digitized by a 16-bit RFR-01 recorder at (fs=10) kHz. The resulting phasors were processed using the same Python algorithm as in the Monte Carlo simulations.

Under natural measurement uncertainty of approximately 0.8–1.2% in amplitude and ±3–4° in phase, the experimental results were compared with Monte Carlo simulations using 1% amplitude and ±5° phase noise. The mean relative fault-location errors were 3.13% and 4.07%, respectively, with a mean absolute difference of 0.056 km (0.93%), as shown in Table 3.

Table 3. Comparison of Monte Carlo simulation and physical experiment results

Test	R_F (Ω)	L_{FL} (km)	l_{estMC} (km)	$Error_{MC}$ (%)	l_{estExp} (km)	$Error_{Exp}$ (%)	$\lvert\Delta l_{MC-Exp}\rvert$ (km)
1	0	6.00	6.02	0.33	6.0	0.83	0.03
2	500	6.00	6.08	1.33	6.12	2.00	0.04
3	1000	6.00	6.15	2.50	6.21	3.50	0.06
4	1500	6.00	6.28	4.67	6.35	5.83	0.07
5	2000	6.00	6.41	6.83	6.49	8.17	0.08

The simulation and experimental results show good agreement, with a maximum discrepancy below 0.08 km (1.3%). This supports the adequacy of the distributed ABCD model and the noise assumptions used in the Monte Carlo analysis. At ($R_F = 2000$ Ohm), the experimental error remained below 8.2%, representing a 70–85% reduction compared with conventional lumped-parameter methods under comparable conditions.

Figure 9 shows the relative fault-location error versus (R_F) for both datasets. The error increases from 0.33% to 6.83% in the Monte Carlo simulations and from 0.83% to 8.17% in the physical experiment. The similar trends and maximum difference of 1.34 percentage points are consistent with the agreement reported in Table 3. Overall, the results demonstrate that the proposed iterative method maintains reliable fault-location accuracy under both simulated and experimental conditions for a 35 kV overhead line with an isolated neutral.

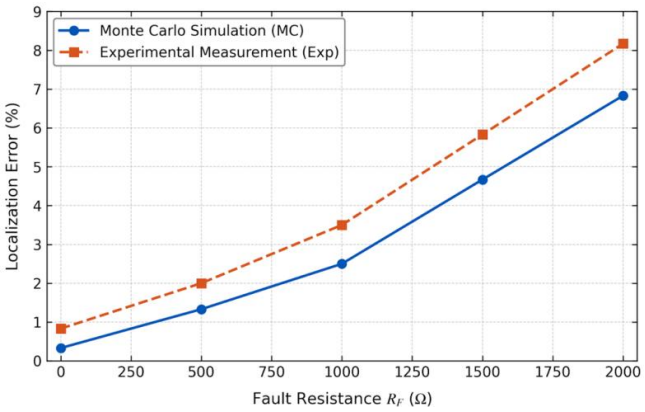


Figure 9. Relative fault-location error versus transition resistance R_F: comparison of Monte Carlo simulations and full-scale physical experiments ((L=12) km, ($l_{true} = 6$) km))

To evaluate the advantages of the developed method based on the ABCD matrix with distributed parameters, a comparison was made with a simplified model with concentrated parameters, in which the distance to failure is estimated as $l_{FL} = \frac{\dot{z}_{in}}{\dot{z}}$ without taking into account distributed capacitances and wave effects, Ohm.

This leads to significant errors in the presence of capacitive current (phase 75-90°), since the model ignores shunt capacitances and assumes a purely inductive-resistive line. The results of the comparison of models with identical model parameters are shown in Table 4.

The lumped model shows a consistently high error (≈50%), regardless of R_F and U, due to the neglect of distributed capacitances, which is critical for 35 kV networks with capacitive current (phase >75°). The developed method reduces the error to an average of 12.4% (70-88% improvement), especially at high R_F (>1000 Ohm), where wave effects and optimization minimize the influence of noise and R_F.

Table 4. Comparison of errors in the lumped model and the developed method for average values of U for each R_F

R_F, Ohm	Phase shift angle φ (°)	Average error using the simplified method, δ_{cp1}, %	Average error based on the ABCD matrix, δ_{cp2}, %	Improvement (%)
400.00	75.00	50.00	16.30	67.40
600.00	76.90	50.00	6.30	87.40
800.00	78.80	50.01	11.90	76.20
1000.00	80.60	50.01	15.60	68.80
1200.00	82.50	50.01	11.50	77.00
1400.00	84.40	50.02	16.30	67.40
1600.00	86.30	50.02	10.20	79.60
1800.00	88.10	50.03	17.90	64.20
2000.00	90.00	50.04	6.20	87.60

This confirms the superiority of the distributed model for lines >10 km, where lumped leads to an underestimation of l_{calc}. For short lines (<5 km), the lumped model may be sufficient, but in general, the

ABCD method is preferable. Table 5 presents a comparison of the selected method with alternative approaches to the task of determining the location of damage in networks with distributed parameters with a voltage of 6(10)-35 kV.

A critical comparison with recent published results contextualizes the proposed method within the broader research landscape. Ensemble-learning approaches [2] report 94–97% accuracy on IEEE 34-node feeders, yet their validation is limited to lumped-parameter test cases with line lengths below 8 km and transition resistance below 500 Ohm; extrapolation to the present conditions (12–50 km, R_F up to 2000 Ohm, isolated neutral) would inevitably degrade their performance due to training-data mismatch. Traveling-wave methods [4], [5] achieve sub-20 m spatial resolution but require sampling rates above 10 kHz and, in some cases, synchronized multi-terminal measurements, rendering them impractical for legacy 6–35 kV overhead networks equipped with standard 0.5-class instrument transformers. The distributed-parameter sparse-estimation framework of [10] confirms the superiority of exact distributed modelling (40–60% error reduction over lumped approaches, consistent with our 70–88% improvement), yet targets high-voltage transmission networks with effectively grounded neutrals and requires multi-terminal PMU data. Methods designed for resonant-grounded systems [12], [13] exploit active current injection from the arc-suppression device, which is absent in isolated-neutral networks; despite this fundamental disadvantage, the proposed method achieves comparable accuracy (mean error 3.13%) to approaches benefiting from active signal injection.

Table 5. Comparative analysis of optimization methods

Method	Error (%)	Computation time	Distributed parameters	R_F influence	Single-ended
1. Classic impedance (lumped)	10-50	<1 ms	No	High sensitivity (underestimation of l)	Yes
2. Traveling-wave methods [4], [5]	5-20 (<20 m)	10-50 ms	Partially	Medium	Mostly no
3. Machine learning (CNN/ensemble) [2], [6], [8]	2-10	<1 ms	No	Medium	Depends
4. Nelder-Mead (Simplex)	5-10	5-200 ms	Possible	Medium	Yes
5. Genetic algorithms	5-10	0.5-5 s	Possible	Medium	Yes
6. Proposed (ABCD iterative)	0-3.5 (avg 3.13)	80-120 ms	Yes (exact)	Minimized (joint l/RF estimation)	Yes

The proposed method has several limitations that define its applicability domain. First, accuracy decreases for short lines (L<20 km), where the receiving-end impedance (Z_{R0}) has a stronger influence on (Z_{in}) and reduces the sensitivity of the inverse problem. The error increases from 7.98% at (L=10) km to 2.11% at (L=50) km (Table 1). Second, under low-voltage conditions U_0<3500 V, the relative error may reach 20–30% because of the reduced signal-to-noise ratio, requiring sufficiently accurate measurement equipment. Third, the Levenberg–Marquardt optimization requires approximately 80–120 ms (12–18 iterations), compared with less than 1 ms for direct algebraic impedance methods. This is acceptable for post-fault analysis and autoreclosing but limits application in ultra-high-speed protection.

The method also requires prior knowledge of the distributed line parameters (z_0) and (y_0). Although the results indicate tolerance to ±20% variation in (C_0), long-term parameter changes may require adaptive identification. The present formulation assumes a radial single-feeder topology; branched networks would require topology-aware extensions. Overall, the most suitable application domain is 20–50 km overhead feeders in 6–35 kV isolated-neutral networks.

Beyond localization accuracy, the proposed method has practical relevance for several modern power-system applications. In smart grid distribution automation, its single-ended operation without dedicated communication links makes it suitable for self-healing and post-fault diagnostic functions, potentially reducing fault restoration time. In IEC 61850-based substations, the algorithm can be implemented on IEDs using zero-sequence measurements supplied by merging units, without requiring additional measurement hardware. The low computational demand (80–120 ms) and limited input data requirements – one voltage and one current channel per feeder – also make the method suitable for edge-based condition monitoring and low-bandwidth communication platforms, including LoRa, NB-IoT, and 5G. In addition, rapid fault-distance estimation without line disconnection can support automatic reclosing and post-fault diagnostics, contributing to improved continuity of distribution service.

4. CONCLUSION

This study developed a single-ended fault-location method for 6–35 kV isolated-neutral networks by combining a distributed ABCD-parameter model with iterative least-squares estimation of fault distance and transition resistance R_F. Monte Carlo simulations and full-scale tests on a 12 km, 35 kV overhead line demonstrated consistent localization performance under capacitive fault-current conditions and high transition resistance. The Monte Carlo analysis yielded a mean relative error of 3.13%, with individual errors ranging from 0.33% to 6.83%, while the experimental results showed a maximum discrepancy of 0.08 km from the corresponding simulation results. These findings indicate that accurate single-ended fault localization can be achieved without line disconnection or synchronized multi-terminal measurements.

The applicability of the method is subject to several limitations. Experimental validation was performed on a single homogeneous overhead line under single-line-to-ground fault conditions. The algorithm also requires prior knowledge of the distributed line parameters, which may change with long-term operating and environmental conditions. In addition, the computational time of 80–120 ms is suitable for post-fault analysis but limits application in ultra-high-speed protection.

Future work will address hybrid physics-based and ML approaches, adaptive identification of distributed line parameters, and validation on branched and ring networks as well as cable and mixed conductor configurations. Further studies will also evaluate the sensitivity of the joint estimation of fault distance and R_F under a wider range of measurement and system uncertainties.

ACKNOWLEDGMENTS

The authors express their gratitude to the administration and technical staff of Akhmet Baitursynuly Kostanay Regional University for providing access to the university's electrical network test site and specialized laboratory equipment, which enabled the successful realization of the full-scale physical experiments for this study.

FUNDING INFORMATION

This research was supported and funded under the internal doctoral development contract and institutional research program of Akhmet Baitursynuly Kostanay Regional University (Project theme: "Development of methods and means for improving the efficiency of fault location in 6(10)–35 kV electrical networks with isolated neutral").

AUTHOR CONTRIBUTIONS STATEMENT

This journal uses the Contributor Roles Taxonomy (CRediT) to recognize individual author contributions, reduce authorship disputes, and facilitate collaboration.

Name of Author	C	M	So	Va	Fo	I	R	D	O	E	Vi	Su	P	Fu
Uspanova Anastasia Igorevna	✓	✓		✓	✓	✓	✓	✓	✓	✓	✓	✓	✓	✓
Sheryazov Saken Koishybaevich	✓			✓	✓					✓		✓	✓	
Koshkin Igor Vladimirovich	✓	✓	✓	✓		✓			✓	✓				
Uspanov Azamat Akhmetuly	✓		✓	✓			✓	✓	✓		✓			✓
Utegulov Arman Bolatbekovich	✓				✓	✓	✓		✓	✓			✓	✓

C : **C**onceptualization
M : **M**ethodology
So : **So**ftware
Va : **Va**lidation
Fo : **Fo**rmal analysis
I : **I**nvestigation
R : **R**esources
D : **D**ata Curation
O : Writing - **O**riginal Draft
E : Writing - Review & **E**diting
Vi : **Vi**sualization
Su : **Su**pervision
P : **P**roject administration
Fu : **Fu**nding acquisition

CONFLICT OF INTEREST STATEMENT

The authors declare that there is no conflict of interest regarding the publication of this article. The authors have no competing financial interests or personal relationships that could have appeared to influence the work reported in this paper.

DATA AVAILABILITY

The authors confirm that all data supporting the findings, simulation parameters, and experimental results of this study are fully available within the article.

REFERENCES

[1] M. M. Saha, J. Izykowski, and E. Rosolowski, *Fault location on power networks*. London: Springer London, 2010, doi: 10.1007/978-1-84882-886-5.

[2] H. Okumus, F. M. Nuroglu, and S. McLoone, "Ensemble learning for short circuit fault location estimation in distribution networks," *Engineering Applications of Artificial Intelligence*, vol. 159, Nov. 2025, doi: 10.1016/j.engappai.2025.111640.

[3] R. Kumar and D. Saxena, "A Hybrid scheme for fault location in unbalanced multi-lateral distribution network with distributed generation," *Computers & Electrical Engineering*, vol. 93, Jul. 2021, doi: 10.1016/j.compeleceng.2021.107301.

[4] G. Pathirage, R. Razzaghi, and L. Andrew, "Fault location in power distribution networks using frequency analysis of traveling waves," *Electric Power Systems Research*, vol. 249, Dec. 2025, doi: 10.1016/j.epsr.2025.111971.

[5] F. Deng, Z. Wang, Y. Chen, and J. Liu, "Topology-adaptive ground fault location method for distribution networks," *International Journal of Electrical Power & Energy Systems*, vol. 176, Mar. 2026, doi: 10.1016/j.ijepes.2026.111675.

[6] T. Yildiz and A. Abur, "Convolutional neural network-assisted fault detection and location using few PMUs," *Electric Power Systems Research*, vol. 235, Oct. 2024, doi: 10.1016/j.epsr.2024.110705.

[7] Z. Wang, X. Ma, Y. Lu, C. Wang, X. Lin, and Q. Sui, "Single-ended data based fault location method for multi-branch distribution network," *Energy Reports*, vol. 6, pp. 385–390, Feb. 2020, doi: 10.1016/j.egyr.2019.11.092.

[8] S. S. Koyshybaevich, U. A. Igorevna, J. Titko, K. I. Vladimirovich, and U. A. Bolatbekovich, "Modeling 6(10)-35 kV electrical network for fault location via negative correlation," *Bulletin of Electrical Engineering and Informatics*, vol. 14, no. 1, pp. 60–72, Feb. 2025, doi: 10.11591/eei.v14i1.7544.

[9] Q. Pang, L. Ye, H. Gao, X. Li, Y. Wang, and T. Cao, "Multi-timescale-based fault section location in distribution networks," *IEEE Access*, vol. 9, pp. 148698–148709, 2021, doi: 10.1109/ACCESS.2021.3123180.

[10] Y. Jia, Y. Liu, B. Wang, D. Lu, and Y. Lin, "Power network fault location with exact distributed parameter line model and sparse estimation," *Electric Power Systems Research*, vol. 212, Nov. 2022, doi: 10.1016/j.epsr.2022.108137.

[11] L. Rui, P. Nan, Y. Zhi, and F. Zare, "A novel single-phase-to-earth fault location method for distribution network based on zero-sequence components distribution characteristics," *International Journal of Electrical Power & Energy Systems*, vol. 102, pp. 11–22, Nov. 2018, doi: 10.1016/j.ijepes.2018.04.015.

[12] J. Qiao, X. Yin, Y. Wang, W. Xu, and L. Tan, "An accurate fault location method for distribution network based on active transfer arc-suppression device," *Energy Reports*, vol. 7, pp. 552–560, Nov. 2021, doi: 10.1016/j.egyr.2021.08.006.

[13] F. Deng *et al.*, "A method for distribution network line selection and fault location based on a hierarchical fault monitoring and control system," *International Journal of Electrical Power & Energy Systems*, vol. 123, Dec. 2020, doi: 10.1016/j.ijepes.2020.106061.

[14] Z. Li *et al.*, "Single-phase-to-ground fault section location in flexible resonant grounding distribution networks using soft open points," *International Journal of Electrical Power & Energy Systems*, vol. 122, Nov. 2020, doi: 10.1016/j.ijepes.2020.106198.

[15] V. Kachesov, A. Lebedev, and E. Kitova, "Monitoring in 6–35 kV power networks, location of single-phase ground fault and detection of fault feeder," *International Journal of Electrical Power & Energy Systems*, vol. 152, Oct. 2023, doi: 10.1016/j.ijepes.2023.109271.

[16] H. Wang, Y. Liu, S. Li, H. Yu, and J. Bian, "Fault section location method for DC distribution networks based on sparse representation of current modal components," *Measurement*, vol. 253, Sep. 2025, doi: 10.1016/j.measurement.2025.117593.

[17] X. Xie, Z. Gao, J. Zhang, and Z. Wang, "A fault location method based on cause-effect network in active distribution network," in *2019 IEEE 8th Joint International Information Technology and Artificial Intelligence Conference (ITAIC)*, 2019, pp. 837–842, doi: 10.1109/ITAIC.2019.8785561.

[18] L. A. Slavutskii and N. N. Ivanova, "Using the simplest neural network as a tool for fault location in power lines," in *AIP Conference Proceedings*, 2022, doi: 10.1063/5.0074926.

[19] B. Li, L. Tang, Z. Gu, L. Liu, and Z. Wu, "Research on distribution network fault location based on electric field coupling voltage sensing and multi-source information fusion," *Energies*, vol. 18, no. 4, Feb. 2025, doi: 10.3390/en18040913.

[20] C. C. Ukwuoma *et al.*, "Power transmission system's fault location, detection, and classification: Pay close attention to transmission nodes," *International Journal of Electrical Power & Energy Systems*, vol. 156, Feb. 2024, doi: 10.1016/j.ijepes.2023.109771.

[21] M. Dashtdar, R. Dashti, and H. R. Shaker, "Distribution network fault section identification and fault location using artificial neural network," in *2018 5th International Conference on Electrical and Electronic Engineering (ICEEE)*, May 2018, pp. 273–278, doi: 10.1109/ICEEE2.2018.8391345.

[22] W. Zi, W. Liu, L. Cheng, and D. Zou, "Fault location method of active distribution networks based on graph attention V2 network," in *2024 China International Conference on Electricity Distribution (CICED)*, 2024, pp. 1134–1139, doi: 10.1109/CICED63421.2024.10753856.

[23] D. Konane, W. Y. S. B. Ouedraogo, T. T. Guingane, A. Zongo, Z. Koalaga, and F. Zougmoré, "An exact solution of telegraph equations for voltage monitoring of electrical transmission line," *Energy and Power Engineering*, vol. 14, no. 11, pp. 669–679, 2022, doi: 10.4236/epe.2022.1411036.

[24] S. Kühn, "General analytic solution of the telegrapher's equations and the resulting consequences for electrically short transmission lines," *Journal of Electromagnetic Analysis and Applications*, vol. 12, no. 06, pp. 71–87, 2020, doi: 10.4236/jemaa.2020.126007.

[25] E. Zio, M. Delfanti, L. Giorgi, V. Olivieri, and G. Sansavini, "Monte carlo simulation-based probabilistic assessment of DG

penetration in medium voltage distribution networks," *International Journal of Electrical Power & Energy Systems*, vol. 64, pp. 852–860, Jan. 2015, doi: 10.1016/j.ijepes.2014.08.004.

BIOGRAPHIES OF AUTHORS



Uspanova Anastasia Igorevna she received her higher education in 2013-2017 at Kostanay State University named after A. Baitursynov with a degree in technology in the field of energy. Received a master's degree in 2017-2019 with a degree in "Master of Engineering and Technology" in the field of technology and equipment. She is currently a senior lecturer in the Department of Mathematics and Physics and a doctoral candidate in the Electric Power Engineering program at Akhmet Baitursynuly Kostanay Regional University. Her research interests include renewable energy, automation and relay protection of electrical grid elements, and power electronics. She can be contacted at email: kamorrasweet1@gmail.com.



Sheryazov Saken Koishybaevich Doctor of Technical Sciences, professor, was born on October 12, 1960, in Kazakhstan. He has over 40 years of scientific and pedagogical experience. He is the head of the scientific school "Improving the Efficiency of Energy Supply for Enterprises Using Renewable Energy Sources," and conducts research in the field of improving efficiency and energy conservation in the electricity supply system. He is the author of over 350 scientific papers, 7 monographs, and more than 25 patents in the field of energy and renewable energy sources. He is a doctoral supervisor, an international accreditation expert (IQAA), a permanent member of two dissertation councils, a member of the editorial board, and a reviewer for highly ranked scientific publications. He can be contacted at email: sakenu@yandex.ru.



Koshkin Igor Vladimirovich born in 1973 in the city of Kostanay, Kazakhstan. In 1997, he graduated from the Kostanay Agricultural Institute with a degree in "Power Supply and Electrification of Agriculture." In 2007, he successfully defended his thesis for the degree of Candidate of Technical Sciences in Electrical Equipment and Electrical Technologies in Agriculture at the Kazakh National Agrarian University in Almaty, Kazakhstan. Since 2011, he has been working as the head of the Department of Electrical Power Engineering at the Akhmet Baitursynov Kostanay Regional University in Kostanay, Kazakhstan. Her research interests include the design of micro-energy systems with renewable energy sources, energy conservation and climate change, and the automation of power supply systems. He can be contacted at email: elektroenergetika330@gmail.com.



Uspanov Azamat Akhmetuly was born in 1998 in Kostanay, Kazakhstan. From 2016 to 2020, he studied at A. Baitursynov Kostanay State University, where he received a Bachelor's degree in Information and Communication Technology, specializing in Computing Systems and Software. Following his undergraduate studies, from 2020 to 2022, he continued his education at A. Baitursynov Kostanay Regional University, earning a Master's degree in Technical Sciences in the "Computer Linguistics" educational program with a scientific-pedagogical focus. Currently, he works as a programmer at the Center of Excellence of the Autonomous Educational Organization "Nazarbayev Intellectual Schools" (AEO NIS) and is also pursuing a doctoral degree in the educational program "Electric Power Engineering". He can be contacted at email: 11w4pfb5h@gmail.com.



Utegulov Arman Bolatbekovich associate professor of the Department of Power Supply at the S. Seifullin Kazakh Agrotechnical Research University. He is the author of 210 scientific and methodological works, including 2 innovation patents, 3 methodological manuals, and 1 co-authored monograph. He currently serves as Leading Researcher on the research project "Development of Innovative Technologies for Improving the Efficiency of 6 kV Power Plants to Meet Their Own Needs," funded by grants from the Ministry of Education and Science of the Republic of Kazakhstan. His research interests include power supply, information technologies, and modeling. He can be contacted at email: Arman.Utegulov1976@gmail.com.